

# A high-resolution CMOS imaging detector for the search of neutrinoless double beta decay in $^{82}\text{Se}$

A.E. Chavarria,<sup>1, a</sup> C. Galbiati,<sup>2, 3, 4</sup> X. Li,<sup>2</sup> and J.A. Rowlands<sup>5</sup>

<sup>1</sup>*Kavli Institute for Cosmological Physics and The Enrico Fermi Institute,  
The University of Chicago, Chicago, IL, United States*

<sup>2</sup>*Department of Physics, Princeton University, Princeton, NJ, United States*

<sup>3</sup>*APC, Université Paris Diderot, CNRS/IN2P3, CEA/Irfu, Obs de Paris, USPC, Paris, France*

<sup>4</sup>*Università degli Studi and INFN Cagliari, Cagliari, Italy*

<sup>5</sup>*Division of Physical Sciences, Sunnybrook Health Science Centre, University of Toronto, Toronto, ON, Canada*

(Dated: April 16, 2023)

We introduce a new technology of detectors for the search of the neutrinoless double beta decay of  $^{82}\text{Se}$ . Based on the present literature, imaging devices from amorphous  $^{82}\text{Se}$  evaporated on a complementary metal-oxide-semiconductor (CMOS) active pixel array are expected to have the energy and spatial resolution to produce two-dimensional images of ionizing tracks of utmost quality, effectively akin to an electronic bubble chamber in the double beta decay energy regime. Still to be experimentally demonstrated, a detector consisting of a large array of these devices could have very low backgrounds, possibly reaching  $1 \times 10^{-7}/(\text{kg y})$  in the neutrinoless decay region of interest (ROI), as it may be required for the full exploration of the neutrinoless double beta decay parameter space in the most unfavorable condition of a strongly quenched nucleon axial coupling constant.

PACS numbers: Neutrinos, Double Beta Decay, Dirac and Majorana Fermions

The study of double beta decay is a unique method of inquiry into the nature of neutrinos, as the observation of a neutrinoless branching ratio is the only known avenue to establish that neutrinos are Majorana fermions as opposed to Dirac fermions [1–6].

Recent results on the nuclear physics of the decay [7] highlighted the very elusive nature of this transition: for the case of a normal hierarchy of neutrino masses and a strongly quenched nucleon axial coupling constant<sup>1</sup>, a complete program for the discovery of neutrinoless double beta decay, reaching the Majorana neutrino mass ( $m_{\beta\beta}$ ) of  $1 \text{ meV}/c^2$ , requires the collection of an exposure of  $O(1 \times 10^7 \text{ kg y})$  in a background-free mode.

Following the notation of [8], the background-free condition can be expressed as:

$$M \cdot T \cdot B \cdot \Delta \leq 1, \quad (1)$$

where  $M$  is the isotope mass,  $T$  is the measurement time,  $B$  is the background rate per unit mass, energy and time about the  $Q$ -value of the decay ( $Q_{\beta\beta}$ ), and  $\Delta$  is the full width at half maximum (FWHM) of the energy response at  $Q_{\beta\beta}$ . Considering the required exposure (*i.e.*,  $M \cdot T$ ) cited above, the background-free condition is equivalent to the requirement:

$$B \cdot \Delta \leq 1 \times 10^{-7}/(\text{kg y}). \quad (2)$$

Values of  $B \cdot \Delta$  for currently operating and future proposed experiments are at least four orders of magnitude higher than this value, see Table 7 in Ref. [8] for a review.

We aim to develop imaging detectors from amorphous  $^{82}\text{Se}$  evaporated on a complementary metal-oxide-semiconductor (CMOS) active pixel array. Such devices will have the capability to image with high spatial and energy resolution the mm-long ionization tracks produced by minimum ionizing electrons emitted in the double-beta decay of  $^{82}\text{Se}$ . We present estimates on the expected backgrounds for a large imaging detector deployed in a low-radioactivity environment and show that the proposed technology combines at once the possibility of a low-background implementation, the precise energy resolution required to reject background from the two-neutrino double beta decay channel and the efficient determination of the event topology necessary for a powerful rejection of residual  $\gamma$ -ray background. While not yet experimentally proven, the proposed detector embodies elements that could allow to achieve the background-free requirement set by Eq. 2.

The isotope  $^{82}\text{Se}$  is a good candidate for the search of neutrinoless double beta decay [9–11] due to its high  $Q_{\beta\beta} = 2998 \text{ keV}$  [12] and relatively long two-neutrino double beta decay half-life of  $T_{1/2}^{2\nu} = 1 \times 10^{20} \text{ y}$  [10]. The high  $Q_{\beta\beta}$  leads to a favorable phase-space factor and is significantly above most interfering  $\gamma$ -ray lines from the uranium and thorium decay chains of natural radioactivity, while the long  $T_{1/2}^{2\nu}$  leads to a small contribution of two-neutrino double electron events near  $Q_{\beta\beta}$ . In addition, selenium can form a wide variety of gases that allow for isotopic enrichment by centrifugation [13] or, potentially, at larger scales by distillation [14].

Selenium is a well-established photoconductor commonly used as an X-ray converter in flat panel detectors employed in the medical industry for radiographic and

<sup>1</sup> The strongly quenched nucleon axial coupling constant is phenomenologically parameterized in Ref. [7] as  $g_{\text{phen.}} = 1.269 \times A^{-0.18}$ , where  $A$  is the mass number.

fluoroscopic imaging [15–17]. These detectors feature a thin-film transistor (TFT) pixel array on which a layer of amorphous selenium is evaporated. In turn, a thin metal electrode is deposited on the back of the device to apply an electric field across the selenium. Charge carriers produced by ionizing radiation in the selenium are drifted toward the pixel array, where the charge is stored by a small capacitance on the pixel. Current TFT technology is limited by the relatively large pixel readout noise of  $\sim 1000 e^-$  (charge carriers) [16].

The noise can be readily improved by replacing the TFT array with a CMOS active pixel array. Current CMOS technology has demonstrated pixel noise as low as a few  $e^-$  with pixel sizes as small as tens of  $\mu\text{m}^2$  [18–20]. Imaging areas of hundreds of  $\text{cm}^2$  can be fabricated by standard processing of 200 mm (8 in) diameter silicon wafers at a rate of up to  $1 \times 10^5$  per month by modern silicon foundries. Amorphous selenium layers up to 1 mm thick are standard in the medical industry and will amount to up to 100 g of  $^{82}\text{Se}$  in a CMOS imager fabricated with isotopically enriched selenium. Readout and digitization of the pixel signal can be performed on-board, simplifying the electronics as the data will be directly downloaded from each device. Ancillary infrastructure requirements will be minimal as the devices can be operated at room temperature.

A large array of imagers can be deployed in an underground laboratory within a highly efficient cosmic ray veto [21] for the backgrounds in the energy region of interest (ROI) about  $Q_{\beta\beta}$  to be dominated by radioactive contamination in the inner detector components.

The devices will resolve with high spatial resolution individual energy depositions. A two-dimensional projection of the ionization density of particle tracks occurring within  $\sim 1$  s exposures will be imaged on the plane of the pixel array. The contributions in the ROI from  $\alpha$ 's and  $\beta$ 's emitted by the decay of uranium, thorium and their daughters in the bulk selenium or on the surfaces of the imagers will be suppressed to a negligible level by the established discrimination techniques to reject events from  $\alpha$ -decay by their distinct topology and sequences of radioactive decay by spatial correlations [22]. The main contribution to single electron backgrounds in the ROI will be electrons from interactions of long-range  $\gamma$ -rays emitted by the daughters  $^{214}\text{Bi}$  and  $^{208}\text{Tl}$  in the imagers, which cannot be effectively vetoed by time correlations with the primary short-range radiation due to the coarse time resolution of the devices. Other radioactive isotopes in the bulk selenium with  $Q$ -values above  $Q_{\beta\beta}$  that may offer sub-dominant contributions to the background rate in the ROI are the long-lived cosmogenic isotope  $^{56}\text{Co}$ , and in-situ cosmogenic activation of  $^{83}\text{Se}$  and  $^{78,80,81,82}\text{As}$ .

Other potential sources of  $\gamma$ -rays include the decays of  $^{214}\text{Bi}$ ,  $^{208}\text{Tl}$  and cosmogenic isotopes in the detector components other than the imagers, as well as high-energy

$\gamma$ -rays emitted following neutron capture in the detector. We expect to suppress these backgrounds by the appropriate selection and handling of construction materials to achieve activities of  $^{214}\text{Bi}$ ,  $^{208}\text{Tl}$  and cosmogenic isotopes at the same level or lower than in the imagers. Background from  $\gamma$ -rays due to radiogenic neutrons from uranium and thorium decay can also be significantly reduced by the careful selection and arrangement of detector components for most neutrons to be captured without the emission of high-energy  $\gamma$ -rays.

We have performed a Geant4 [23, 24] simulation of a  $^{82}\text{Se}$  CMOS imaging detector making realistic assumptions on the performance of the devices, with pixels  $15 \times 15 \mu\text{m}^2$  in size, a pixel readout noise of  $10 e^-$  and a pixel dynamic range of 70 dB. We assumed a 200  $\mu\text{m}$ -thick amorphous  $^{82}\text{Se}$  layer and the thickness of the pixel array structure and the back electrode to be less than a few  $\mu\text{m}$ 's for the energy loss in dead regions between imagers to have a negligible impact on the energy resolution. The detector consisted of stacks of modules, each made of two back-to-back imagers that share a common electrode to which the high-voltage is applied.

To estimate the detector performance, we implemented full electron tracking and simulated the charge produced by ionization along the electron's path using a Fano model [25]. Data on the intrinsic resolution of amorphous selenium is severely lacking, with measurements and Monte Carlo simulations existing only up to 140 keV [26, 27]. We adopted an average energy for the production of one electron-hole pair of 15 eV, as measured for 140 keV X-rays at an electric field of 30 V/ $\mu\text{m}$  [27], and a value of the Fano factor  $F = 0.6$ , as predicted at this field [28]. From the simulation of the ionization tracks and the instrumental response, followed by clustering and track reconstruction algorithms, we obtained a FWHM of the energy response at  $Q_{\beta\beta}$  of 17 keV.

We first assessed the background from the two-neutrino decay by simulating pairs of electrons from  $^{82}\text{Se}$  double beta decay. For two-neutrino decay, we assumed the measured decay rate of 1.6 mBq/kg [10]. For the neutrinoless decay, we assumed the most unfavorable case, *i.e.*,  $m_{\beta\beta} = 1 \text{ meV}/c^2$  and a strongly quenched axial coupling constant, corresponding to a total signal rate of  $3.0 \times 10^{-7}/(\text{kg y})$ . We simulated a common exposure of  $3 \times 10^{10} \text{ kg y}$  to amass sufficient statistics for the spectra. Initial momenta distributions for both decays were obtained from the DECAY0 program [29]. The result is shown in Fig. 1. Even in this most unfavorable case, the peak from the neutrinoless decay is distinguishable from background from the two-neutrino channel. We defined a FWHM-wide ROI extending from 2993 keV to 3010 keV, selecting the start of the ROI slightly above the crossing point of the two spectra. We determined that 40% of the neutrinoless decays have a reconstructed energy within the ROI, corresponding to a signal rate of

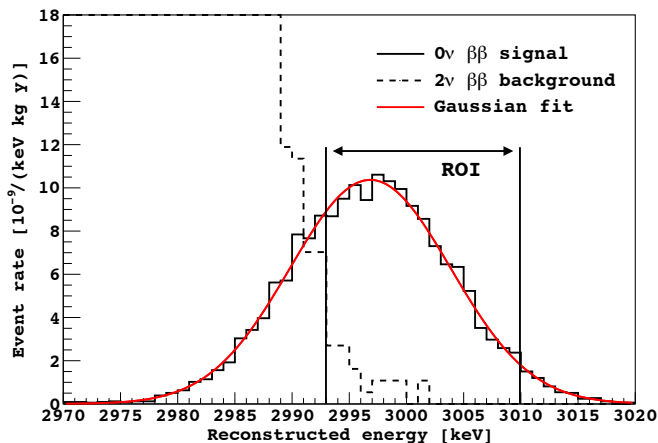


FIG. 1. Reconstructed energy spectrum from simulated neutrinoless ( $0\nu$ ) double beta decay with  $m_{\beta\beta} = 1 \text{ meV}/c^2$  and a strongly quenched axial coupling constant, and two-neutrino ( $2\nu$ ) double beta decay in the amorphous  $^{82}\text{Se}$  imaging detector described in the text. The FWHM-wide ROI for the neutrinoless double beta decay search is labeled.

$1.2 \times 10^{-7}/(\text{kg y})$ . The two-neutrino background has a leakage in the ROI of  $1.2 \times 10^{-8}/(\text{kg y})$ , for a signal to background ratio of 10.

Then we turned to the assessment of background from other sources. We performed a full simulation of the expected electron backgrounds from radioactive decay assuming a bulk contamination in the inner detector of  $^{238}\text{U}$ ,  $^{232}\text{Th}$  and their daughters of  $< 110 \text{ } \mu\text{Bq/kg}$ , as already achieved in enriched  $^{82}\text{Se}$  [13]. For the pixel array we assumed a  $^{238}\text{U}$  and  $^{232}\text{Th}$  contamination of  $< 1 \times 10^{-2} \text{ } \mu\text{Bq/cm}^2$ , and an additional  $^{210}\text{Po}$  surface contamination of  $1 \times 10^{-1} \text{ } \mu\text{Bq/cm}^2$ , as for the charge-coupled devices deployed in the DAMIC experiment [22]. We included the high-energy  $\gamma$ -rays produced by the capture of radiogenic neutrons from fission,  $(\alpha, n)$  reactions of the  $^{238}\text{U}$  and  $^{232}\text{Th}$  decay chains, and  $(\alpha, n)$  reactions of the out-of-equilibrium  $^{210}\text{Po}$  activity. We also considered the contribution in the bulk from cosmogenic  $^{56}\text{Co}$  with an activity of  $< 2 \times 10^{-2} \text{ } \mu\text{Bq/kg}$  [11], as well as activities of  $^{83}\text{Se}$  and  $^{78,80,81,82}\text{As}$  from in-situ cosmogenic production (at a depth of 3800 meters water-equivalent) of  $2 \times 10^{-2} \text{ } \mu\text{Bq/kg}$  and  $3 \times 10^{-4} \text{ } \mu\text{Bq/kg}$ , respectively [30, 31]. The first column in Table I summarizes the total expected rate in the ROI from these background sources. For electrons emitted by  $\beta$ -decay we present the contribution from each class of events described above. For electrons produced by  $\gamma$ -ray interactions, we consider the total  $\gamma$ -ray flux from all background sources and present the contribution by the interaction mechanism.

The electron backgrounds from  $\beta$ -decay will be dominated by  $^{214}\text{Bi}$  and  $^{208}\text{Tl}$  in the bulk and on the surfaces of the imagers, as they are the only daughters from uranium and thorium that can emit electrons (the  $\beta$  par-

ticle and, in some cases, conversion electrons) with total energy in the ROI. The exquisite spatial resolution and dead-time-free operation of the devices will allow to identify these decays within their corresponding decay sequences:  $^{218}\text{Po}$ – $^{214}\text{Pb}$ – $^{214}\text{Bi}$ – $^{214}\text{Po}$  and  $^{216}\text{Po}$ – $^{212}\text{Pb}$ – $^{212}\text{Bi}$ – $^{208}\text{Tl}$ . Considering a probability of missing a single decay in the sequence of  $< 1 \times 10^{-2}$ , a total suppression factor of  $< 1 \times 10^{-6}$  is expected. Likewise, the background rate from the dominant cosmogenic isotope,  $^{83}\text{Se}$ , will be suppressed by a factor  $< 1 \times 10^{-2}$  by its spatial correlation with the subsequent  $\beta$ -decay of  $^{83}\text{Br}$ .

We have investigated the discrimination between single and double electron events by the analysis of their track topologies. The proposed technology will reconstruct in extreme detail any ionizing track: Fig. 2 shows, side by side, the reconstructed images of single electron and double electron events simulated in the ROI. The high quality of the tracks allows to separate, by simple visual examination, single electron tracks, with one Bragg peak, from double electron tracks originating at the same point, with two Bragg peaks. We developed an algorithm based on the increase in straggling and stopping power of the electron at the Bragg peak to identify double electron events and suppress single electron background by  $1 \times 10^{-3}$ . The limitation from this technique arises from single electrons that mimic double electron events by the emission of a  $\delta$ -ray very close to the start of the track, where the emission vertex is indistinguishable from the electron start point. We note that for a detector with an improved spatial resolution of  $5 \times 5 \text{ } \mu\text{m}^2$  this limiting background reduces to  $5 \times 10^{-4}$ .

We have also estimated the discrimination of events based on the spatial correlation with nearby energy depositions in the same exposure. The requirement that the event in the ROI is isolated, *i.e.*, that there are no energy depositions within a 5 cm spherical region

TABLE I. Estimated background rates of minimum-ionizing electron tracks produced by natural radioactivity in the amorphous  $^{82}\text{Se}$  detector of  $15 \times 15 \text{ } \mu\text{m}^2$  pixel size described in the text. The first column specifies the origin of the background. The second column gives the total rate observed in the ROI from the assumed radioactive contaminations. The third column presents the corresponding residual event rates after application of the discrimination criteria.

Radioactive background source	Raw bckg. rate [1/(kg y)]	Rate after discrimination [1/(kg y)]
$\beta$ -decay (bulk)	$< 2.7 \times 10^{-1}$	$< 3.0 \times 10^{-9}$
$\beta$ -decay (surface)	$< 3.3 \times 10^{-1}$	$< 1.0 \times 10^{-8}$
$\beta$ -decay (cosmo.)	$< 8.0 \times 10^{-5}$	$< 1.2 \times 10^{-7}$
$\gamma$ -ray (photo-elec.)	$< 1.0 \times 10^{-3}$	$< 1.0 \times 10^{-6}$
$\gamma$ -ray (Compton)	$< 1.3 \times 10^{-3}$	$< 3.3 \times 10^{-7}$
$\gamma$ -ray (pair prod.)	$< 1.5 \times 10^{-6}$	$< 1.5 \times 10^{-7}$
Total	$< 6.0 \times 10^{-1}$	$< 1.6 \times 10^{-6}$

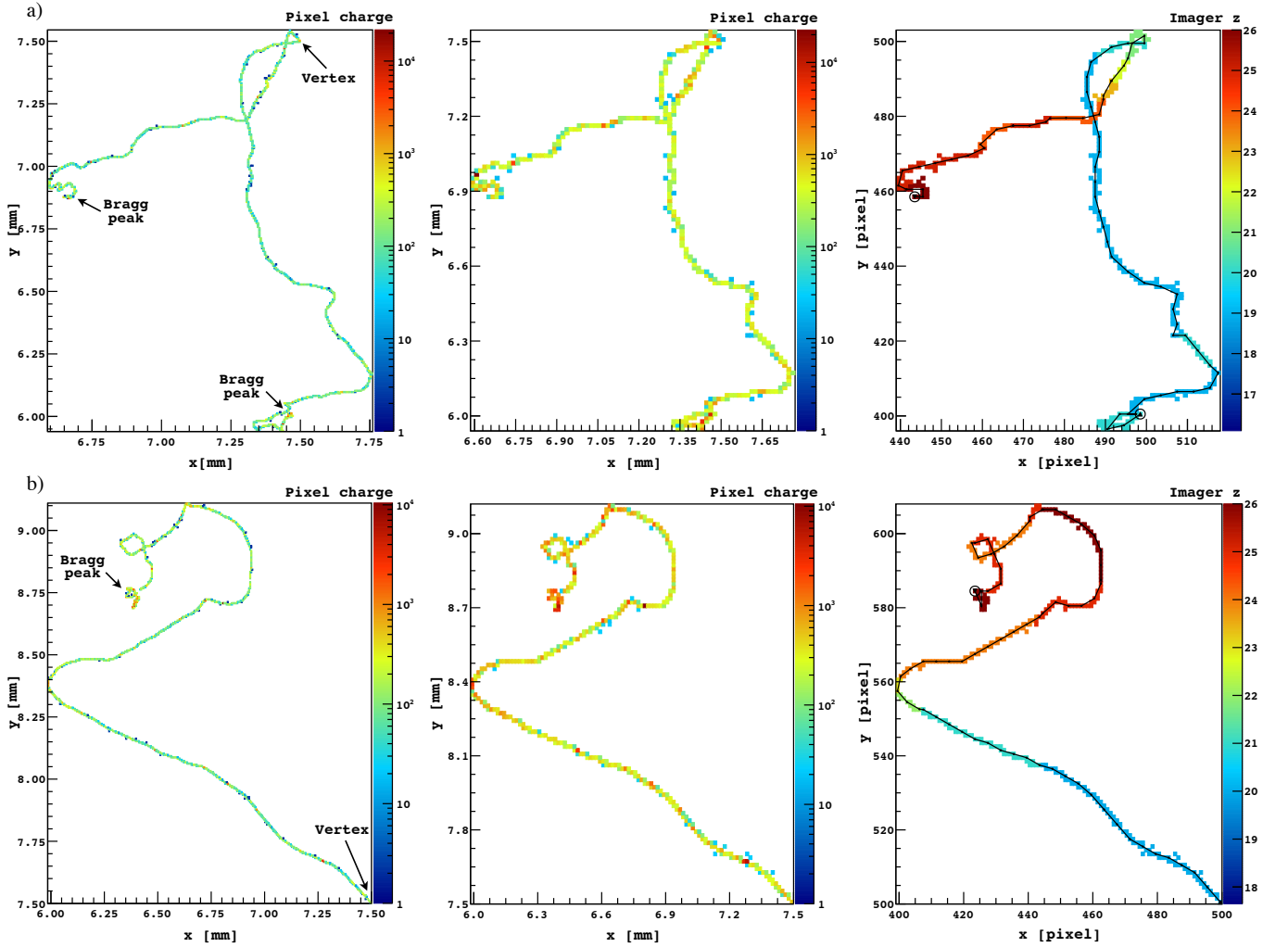


FIG. 2. Double electron (a, top row) and single electron (b, bottom row) simulated events with total energy in the neutrinoless decay ROI. In both cases, the electrons emerge from the single vertex located at coordinates  $(x,y) = (7.5 \text{ mm}, 7.5 \text{ mm})$ . The color axis of the left and middle panels correspond to the number of charge carriers collected by a pixel. The left panel shows the simulated track with a  $5 \times 5 \mu\text{m}^2$  pixel size, while the middle and right panels present the simulated track with  $15 \times 15 \mu\text{m}^2$  technology. The color axis of the right panel corresponds to the identifier of the imager in the stack where the energy deposition took place; higher values represent imagers that are higher up in the stack. The black line shows the reconstructed track for the event, with circles marking where Bragg peaks were identified by the automated algorithm.

of the event, suppresses backgrounds from  $\gamma$ -ray pair-production, Compton scattering of  $\gamma$ -rays with energies  $< 3300 \text{ keV}$ , and  $\beta$ -decay of  $^{214}\text{Bi}$  and  $^{208}\text{Tl}$  with associated  $50 \text{ keV}$  to  $300 \text{ keV}$  photon emission by a factor of  $< 1 \times 10^{-1}$ .

The third column of Table I presents the background for different classes of events after all selection criteria, approaching the ultimate requirement outlined in Eq. 2. The overall acceptance for double beta decay is 50%, dominated by the inefficiency in the selection of events with two Bragg peaks.

The technology introduced in this paper allows for further improvements in background suppression.

Inspired by the mode of operation of bubble chambers [32–35], we explored the possibility to operate the

detector inside a toroidal superconducting magnet to enhance the topological signature of double beta decay events. Fig. 3 shows the tracks of double and single electron events in the ROI in the presence of a 20 T magnetic field: the change in the radius of curvature along the electron track provides a powerful and independent tool to discriminate between double and single electron events, which would improve the acceptance for the double electron signal and give an additional handle on potential backgrounds. It would also provide valuable topological information on events from pair production by high-energy  $\gamma$ -rays.

Additionally, the detector’s imaging capability will allow for the localization of the site of a double beta decay candidate within tens of  $\mu\text{g}$ ’s of selenium in a de-



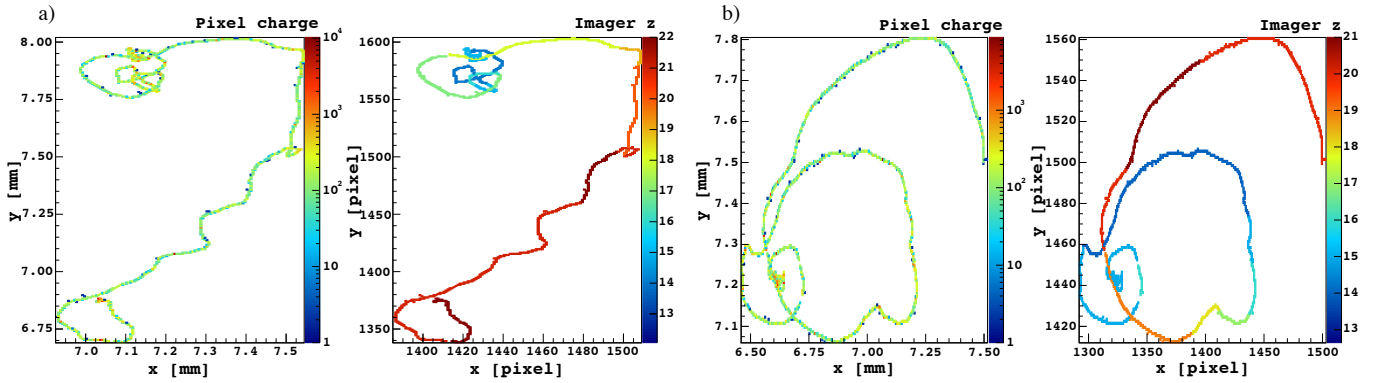


FIG. 3. Double electron (a) and single electron (b) events with vertex  $(x,y) = (7.5 \text{ mm}, 7.5 \text{ mm})$ . The events have been simulated assuming  $5 \times 5 \mu\text{m}^2$  pixel technology and a 20 T magnetic field perpendicular to the plane of the imagers.

tector module. Following the double beta decay of  $^{82}\text{Se}$ , the  $^{82}\text{Kr}$  daughter will remain essentially immobile [36]. Its selective removal and detection by single atom counting [37–39] may be possible and may offer an independent confirmation of double beta decay.

The first step in the experimental program is the design, fabrication and operation of large area, low noise CMOS imagers with amorphous selenium layers of natural isotopic abundance. Characterization of these devices with cosmic rays and radioactive sources in the laboratory will demonstrate the capability to image with high resolution individual ionization tracks, and will allow to measure the intrinsic energy response of amorphous selenium to minimum ionizing particles, determining the average energy for the production of an electron-hole pair and the Fano factor.

A detector, consisting of an array of one hundred imaging modules made from isotopically enriched  $^{82}\text{Se}$ , operated in a shallow underground laboratory, will permit the experimental demonstration of the detector performance outlined in this paper. Ionization tracks from two-neutrino double electron events near  $Q_{\beta\beta}$  and single electrons produced by  $\gamma$ -ray calibration sources will allow to characterize the energy response and topological event discrimination. The uranium and thorium contamination of the imagers and the production cross-sections of cosmogenic isotopes in the  $^{82}\text{Se}$  will also be directly measured. From these results it would be possible to extrapolate to the background expected in the ROI for an extremely large detector operated in a low background environment.

Considering the modular nature of the experiment, its compactness and simplicity in operation, the modest radio-purity requirements, and the scalability of the technology — which relies on widespread fabrication processes in the semiconductor industry — once the required performance is experimentally demonstrated, we would have set the path to a large detector capable of sweeping the parameter space for neutrinoless double beta decay

in the inverted and normal hierarchies of neutrino masses even in the most unfavorable nuclear physics scenarios, likely establishing the fundamental nature of neutrinos.

This work has been supported by the Kavli Institute for Cosmological Physics at the University of Chicago through grant NSF PHY-1125897 and an endowment from the Kavli Foundation, and by Princeton University through grant NSF PHY-1314507. We thank R. Bez, A. Martini, and P. Privitera for discussions and useful comments.

<sup>a</sup> [alvaro@kicp.uchicago.edu](mailto:alvaro@kicp.uchicago.edu)

- [1] P. A. M. Dirac, *Proc. Royal Soc. London A: Math. Phys. Eng. Sci.* **118**, 351 (1928).
- [2] P. A. M. Dirac, *Proc. Royal Soc. London A: Math. Phys. Eng. Sci.* **117**, 610 (1928).
- [3] E. Majorana, *Nuovo Cim.* **14**, 171 (1937).
- [4] M. Goeppert-Mayer, *Phys. Rev.* **48**, 512 (1935).
- [5] W. H. Furry, *Phys. Rev.* **56**, 1184 (1939).
- [6] G. Racah, *Nuovo Cim.* **14**, 322 (1937).
- [7] J. Barea, J. Kotila, and F. Iachello, *Phys. Rev. C* **87**, 014315 (2013).
- [8] S. Dell’Oro, S. Marcocci, M. Viel, and F. Vissani, *Adv High En. Phys.* **2016**, 1 (2016).
- [9] R. Arnold et al., *Nuclear Physics A* **636**, 209 (1998).
- [10] R. Arnold et al., *Nuclear Physics A* **765**, 483 (2006).
- [11] D. R. Artusa et al., *Eur. Phys. J. C* **76**, 364 (2016).
- [12] D. L. Lincoln et al., *Phys. Rev. Lett.* **110**, 012501 (2013).
- [13] J. W. Beeman et al., *Eur. Phys. J. C* **75**, 591 (2015).
- [14] T. R. Mills, B. B. McInteer, and J. G. Montoya (Los Alamos National Laboratory), *Sulfur and selenium isotope separation by distillation*, LA-UR-88-2421, Los Alamos National Laboratory (1988).
- [15] W. Zhao and J. A. Rowlands, *Med. Phys.* **22**, 1595 (1995).
- [16] L. E. Antonuk et al., *Med. Phys.* **27**, 289 (2000).
- [17] D. C. Hunt, O. Tousignant, and J. A. Rowlands, *Med. Phys.* **31**, 1166 (2004).
- [18] M. Bigas, E. Cabruja, J. Forest, and J. Salvi, *Microelectronics Journal* **37**, 433 (2006).

- [19] J.-H. Park et al., *IEEE Trans. Elec. Dev.* **56**, 2414 (2009).
- [20] M.-W. Seo, K. Yasutomi, K. Kagawa, and S. Kawahito, *ITE Trans. MTA* **3**, 258 (2015).
- [21] P. Agnes et al. (The DarkSide collaboration), *JINST* **11**, P03016 (2016).
- [22] A. Aguilar-Arevalo et al., *JINST* **10**, P08014 (2015).
- [23] S. Agostinelli et al., *Nucl. Inst. Meth. A* **506**, 250 (2003).
- [24] J. Allison et al., *IEEE Trans. Nucl. Sci.* **53**, 270 (2006).
- [25] U. Fano, *Phys. Rev.* **72**, 26 (1947).
- [26] Y. Fang et al., *Med. Phys.* **39**, 308 (2012).
- [27] I. M. Blevis, D. C. Hunt, and J. A. Rowlands, *J. Appl. Phys.* **85**, 7958 (1999).
- [28] A. Darbandi, É. Devoie, O. Di Matteo, and O. Rubel, *J. Phys.: Condens. Matter* **24**, 455502 (2012).
- [29] O. A. Ponkratenko, V. I. Tretyak, and Y. G. Zdesenko, *Physics of Atomic Nuclei* **63**, 1282 (2000).
- [30] G. Bellini et al. (The Borexino Collaboration), *JCAP* **1308**, 049 (2013).
- [31] J. B. Albert et al., *JCAP* **2016**, 029 (2016).
- [32] D. A. Glaser, *Phys. Rev.* **87**, 665 (1952).
- [33] F. J. Hasert et al., *Phys. Lett. B* **46**, 121 (1973).
- [34] F. J. Hasert et al., *Phys. Lett. B* **46**, 138 (1973).
- [35] F. J. Hasert et al., *Nucl. Phys. B* **73**, 1 (1974).
- [36] M. J. W. Greuter et al., *J. Appl. Phys.* **77**, 3467 (1995).
- [37] C. Y. Chen et al., *Science* **286**, 1139 (1999).
- [38] X. Du et al., *Geophys. Res. Lett.* **30**, 2068 (2003).
- [39] W. Jiang et al., *Geochimica et Cosmochimica Acta* **91**, 1 (2012).